Atmospheric chemistry and aerosols (II)

Dust in the Martian atmosphere

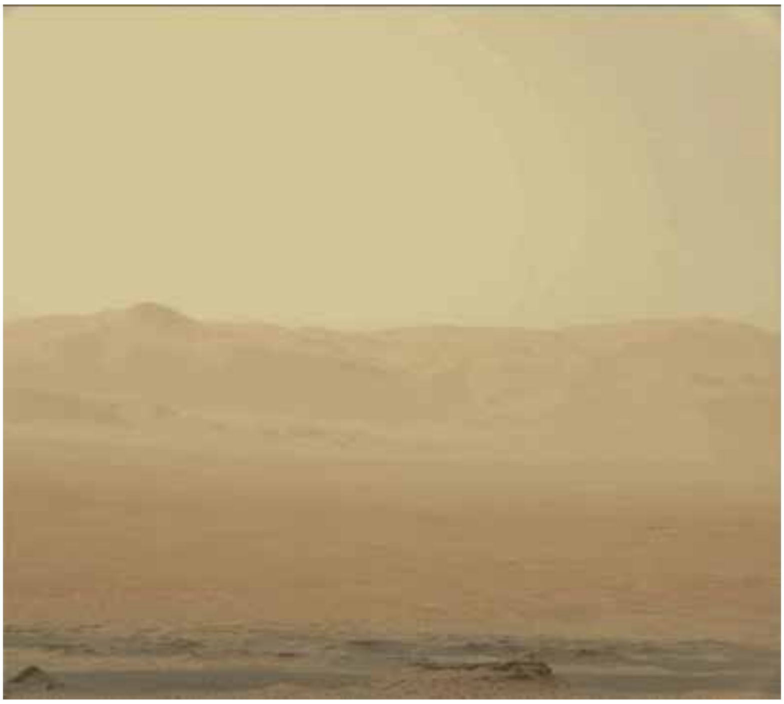

Martian dust storms span the entire planet, in June 2018.
The image was taken from the NASA's rover *Curiosity*

Dust in the Martian atmosphere

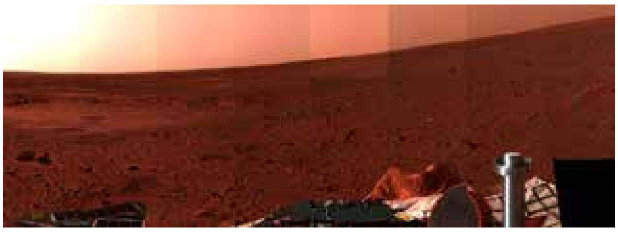

- Micrometer-sized small mineral particles float in the atmosphere with a background optical thickness of 0.1-0.5.
- The dust loading changes with time and space.
- The dust serves as a heat source in the atmosphere by absorbing sunlight.

Seasonal variation of optical thickness in infrared
(Smith et al. 2004)

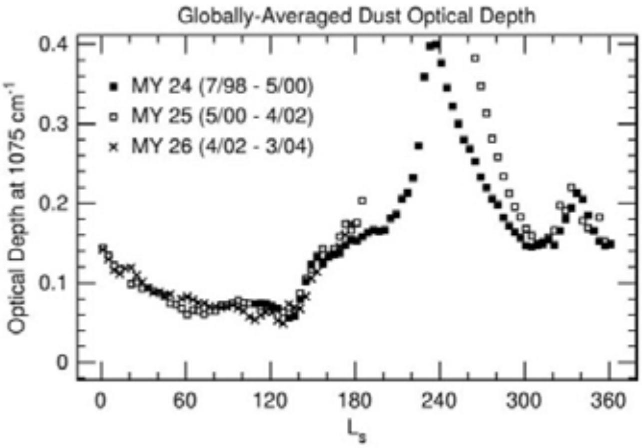

Fig. 7. Globally-averaged daytime (local time ~ 1400) dust optical depth at 1075 cm^{-1} (scaled to an equivalent 6.1-mbar pressure surface) as a function of season (L_s). Three martian years are represented: Mars Year 24 (MY 24) (■), MY 25 (□), MY 26 (×). During the planet-encircling dust storm of 2001 (MY 25), globally-averaged dust opacity reached 1.3 at $L_s = 205$–$215°$.

Seasons of Mars

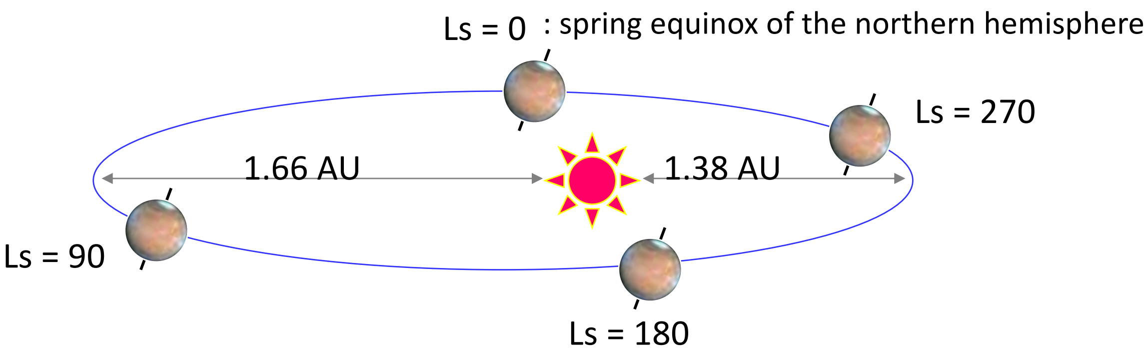

- The north-south asymmetry of the seasonal cycle is large due to the large orbital eccentricity.
- The distance to the sun gets closer in the southern summer.

Dust as a heat source

- Absorption of solar radiation
  - much stronger than the greenhouse effect of CO_2, which is only several kelvins
  - much stronger than cloud albedo effect and latent heat

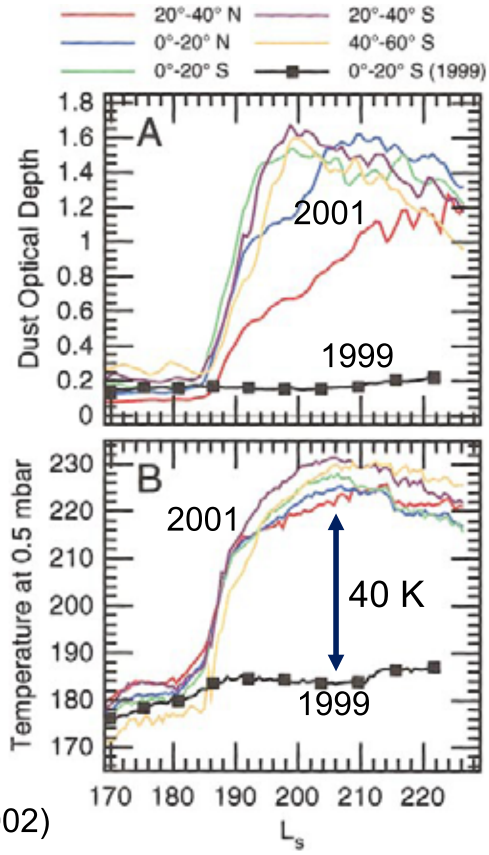

40 K difference between thick-dust year and thin-dust year

Smith et al. (2002)

Dust storms on Mars

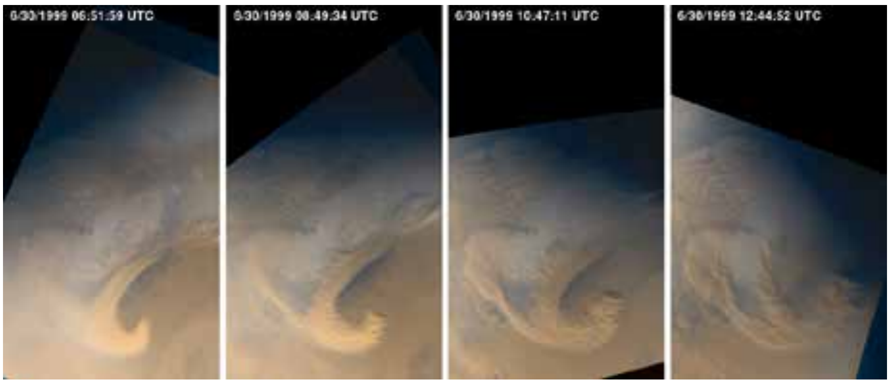

regional storm

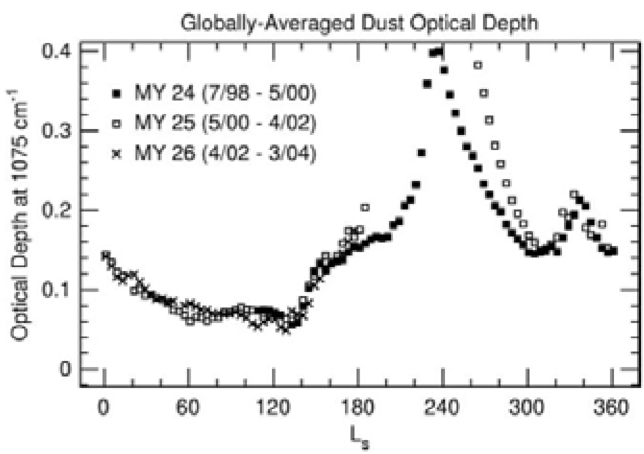

Seasonal variation of optical thickness in infrared
(Smith et al. 2004)

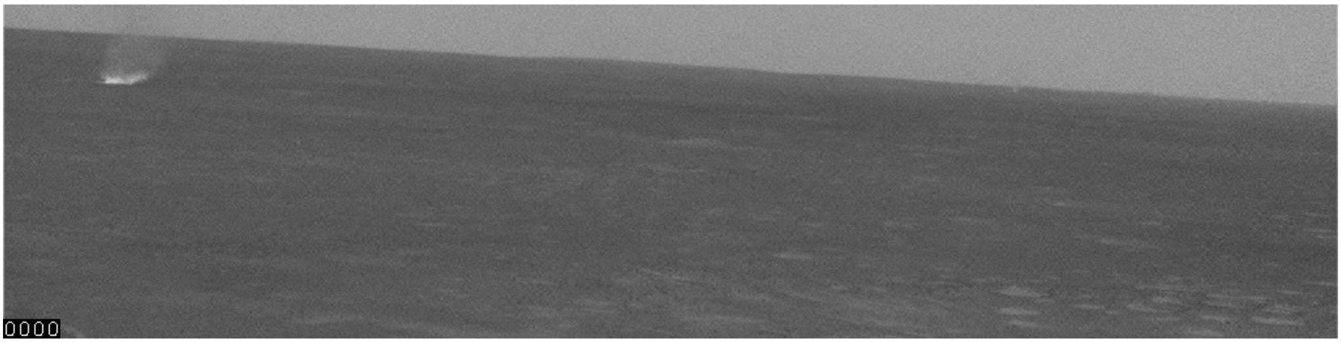

Dust devils

- Source of background atmospheric dust ?

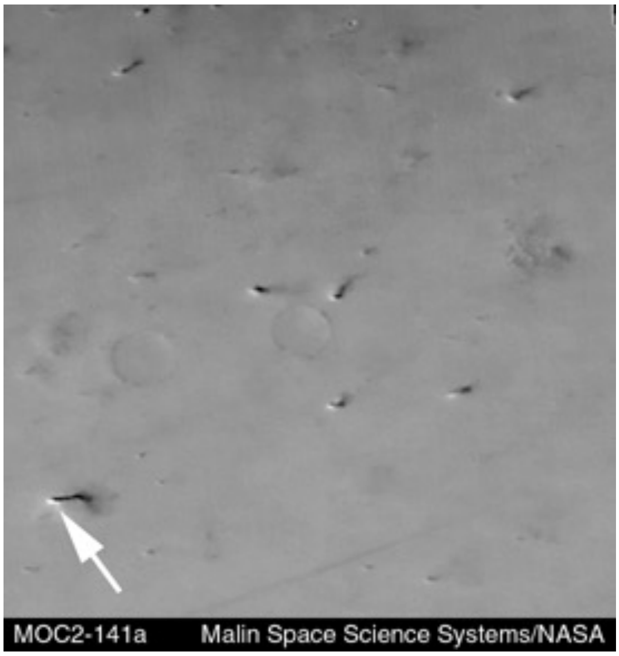

Distribution of atmospheric dust

- Origin of the “background” dust is unknown
- Maximum mixing ratio at 10−20 km altitudes

Smith et al. (2004)

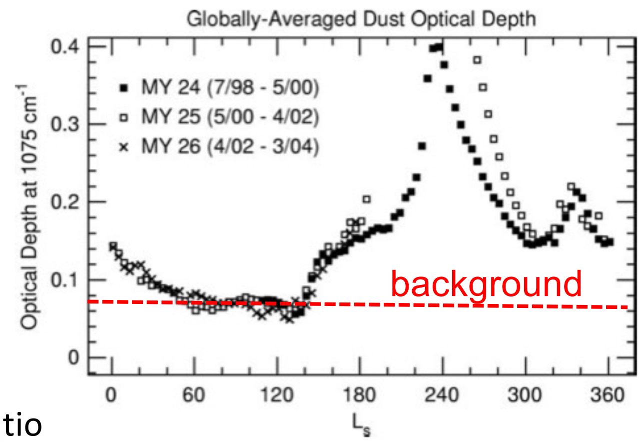

Meridional distribution of dust mixing ratio

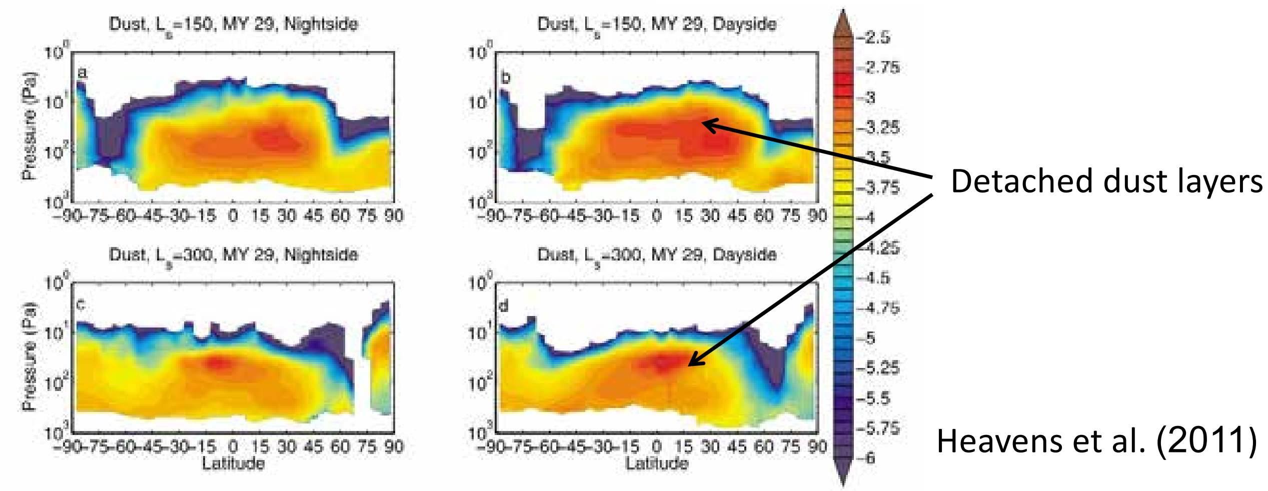

Heavens et al. (2011)

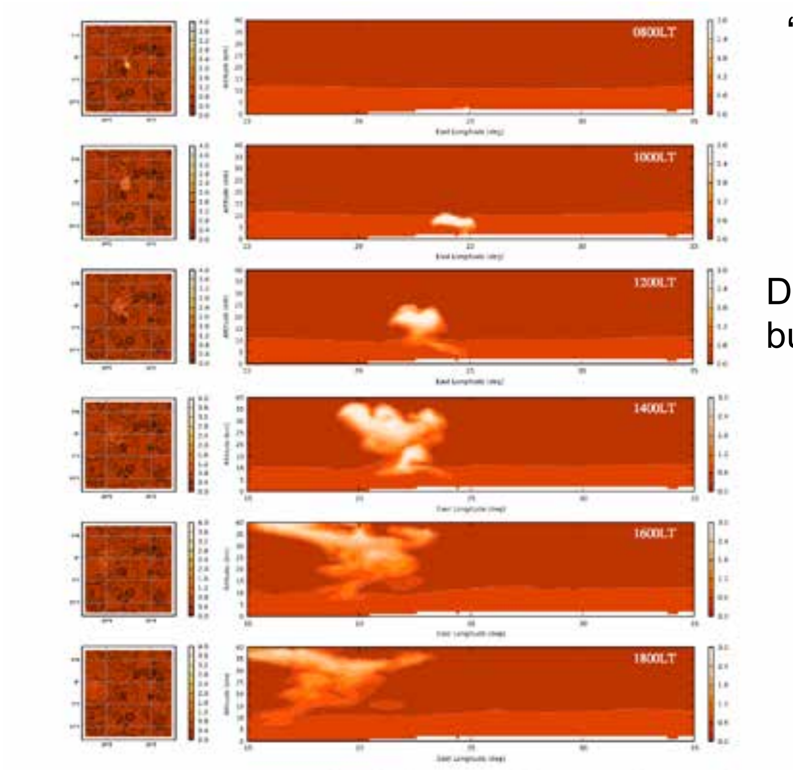

Figure 12. The LMD-MMM storm simulation with lifting and no initial dust perturbation. Same as Figure 4 except that local times range from 0800 to 1800 and longitude-altitude sections are obtained at latitude 1.5°S.

"Rocket dust storm"

Modeling by Spiga et al. (2013)

Dust plumes continuously get buoyancy through solar heating

Global dust storm

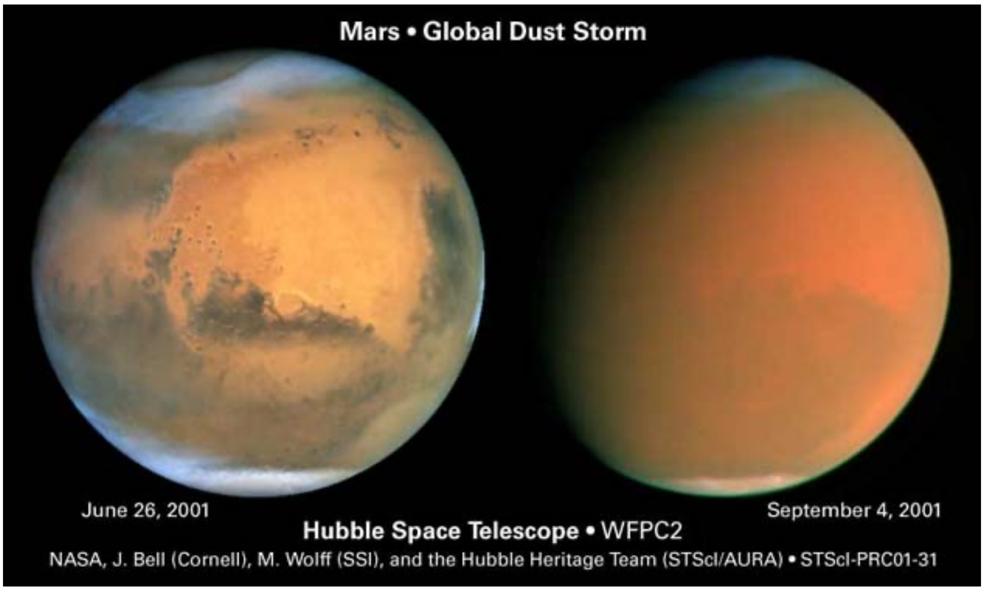

- Global dust storms tend to occur in southern spring-summer
- Positive feedback between dust heating and the intensification of winds is expected in the development of global dust storms.

H_2O ice clouds on Mars

HST Mars image

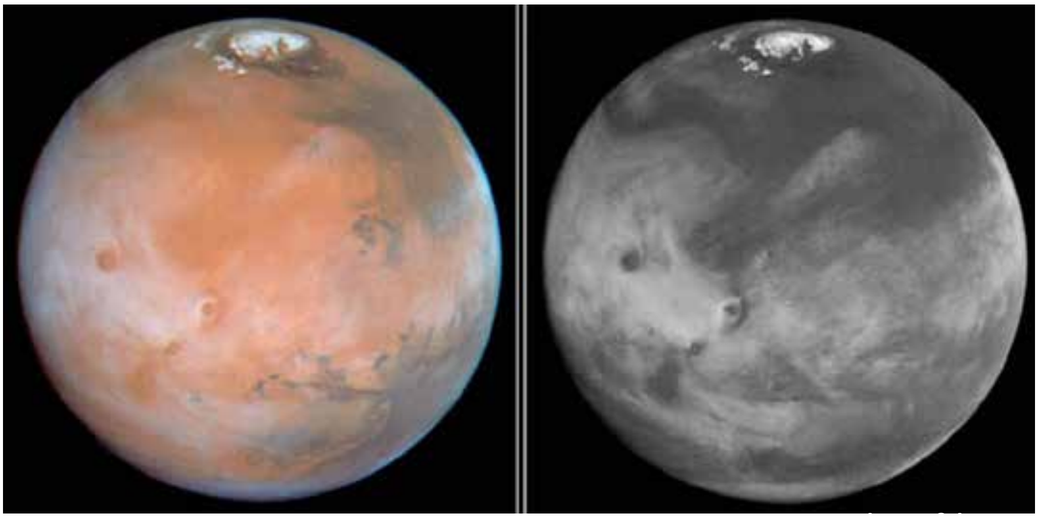

color composite　　blue (410 nm)

Seasonal variation of dust, clouds, and H_2O vapor observed by an infrared spectrometer (TES) on Mars Global Surveyor

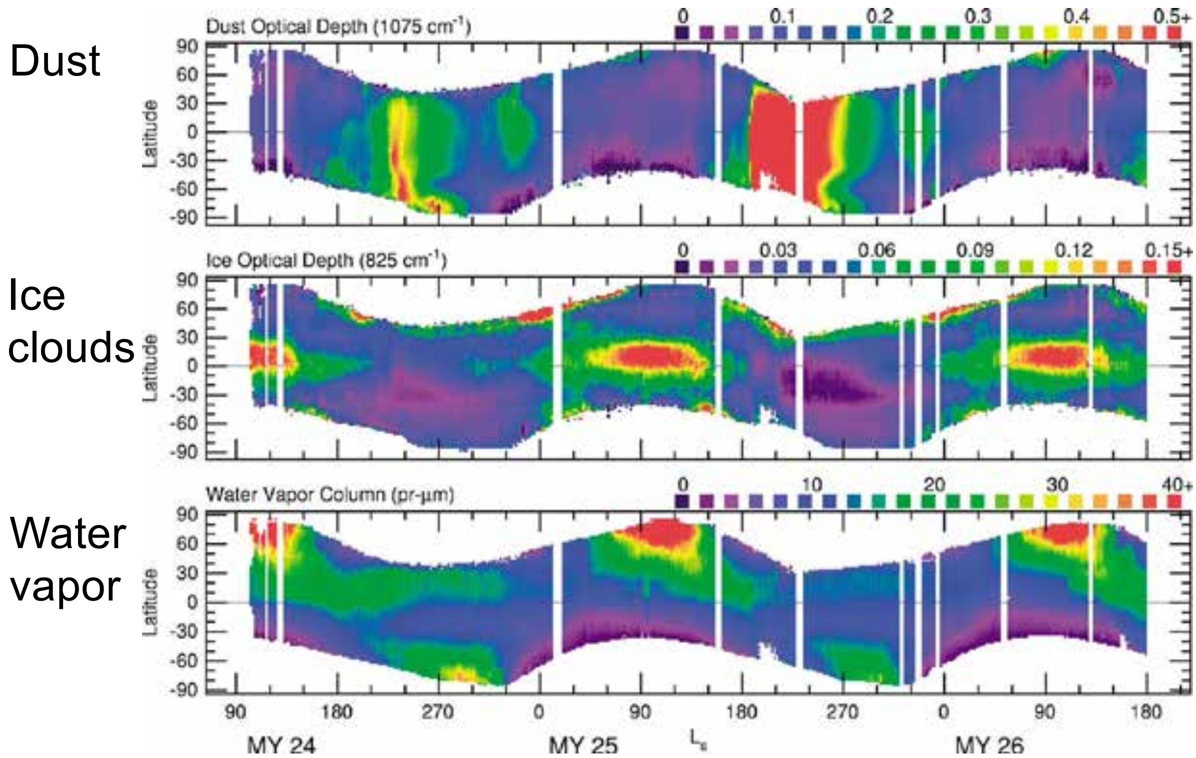

Smith, Icarus 167 (2004) 148–165

Seasonal cycle of Martian water

Water cycle is basically driven by the sublimation from/condensation onto the north polar cap.

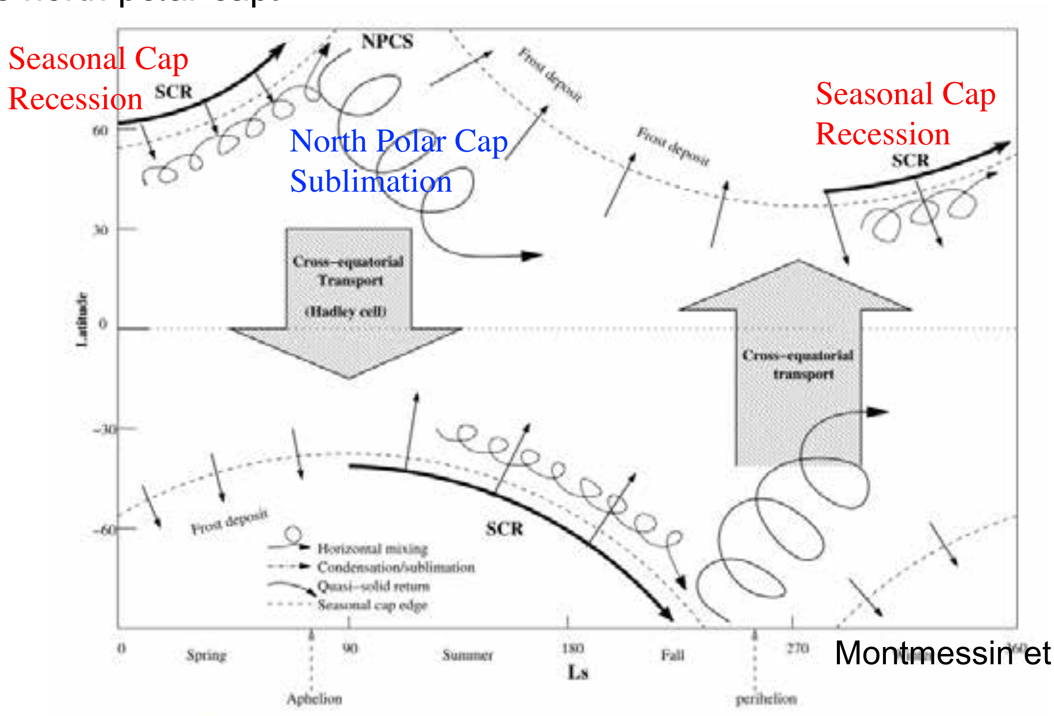

Montmessin et al. (2004)

Figure 3. Chart describing the principal events affecting the Martian water cycle over the course of a year. NPCS stands for North Polar Cap Sublimation; SCR stands for Seasonal Cap Recession.

Polar caps: H_2O ice + CO_2 ice

- Seasonal variation
- Residual polar caps in summer
  - H_2O only on the north
  - H_2O + CO_2 on the south
- Southern CO_2 ice seems to serve as a cold trap of H_2O (Montmessin et al. 2007)

North

South

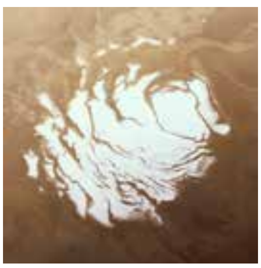

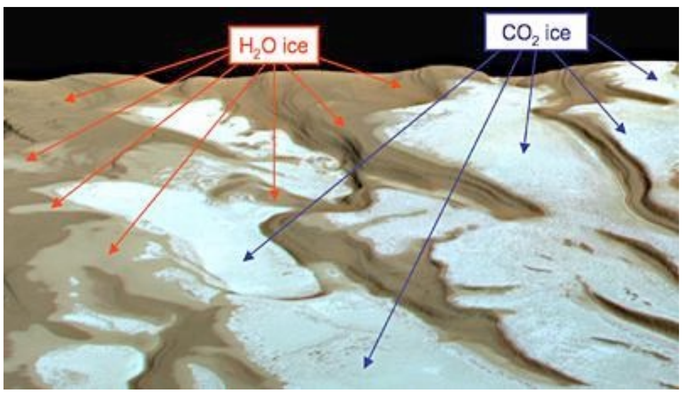

Water transport by Hadley circulation

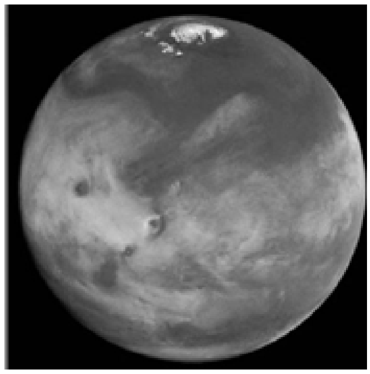

- Warmer southern summer than northern favors net northward transport of water.

H_2O clouds

Distribution of H_2O ice mixing ratio in a Mars GCM

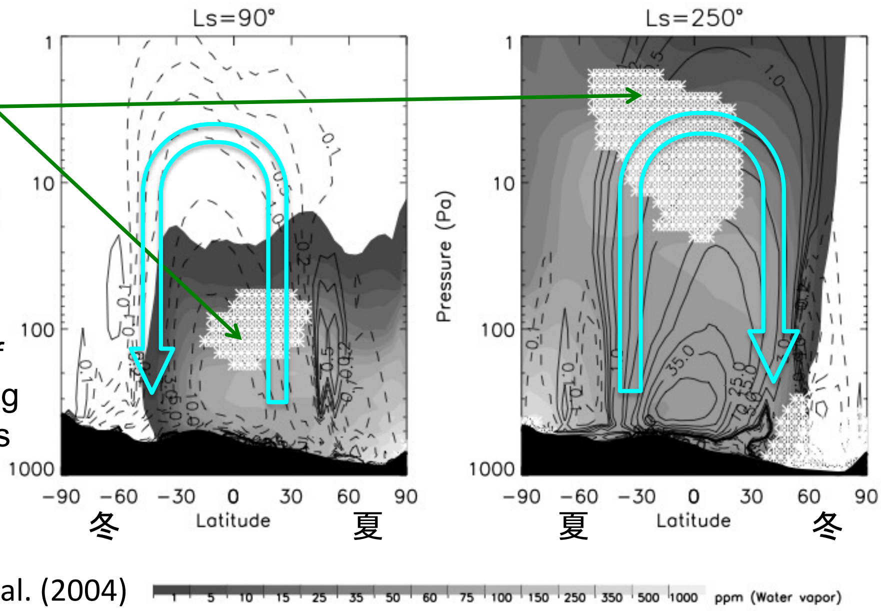

Montmessin et al. (2004)

Supersaturation of water vapor on Mars

SPICAM on Mars Express (Maltagliati et al. 2011)

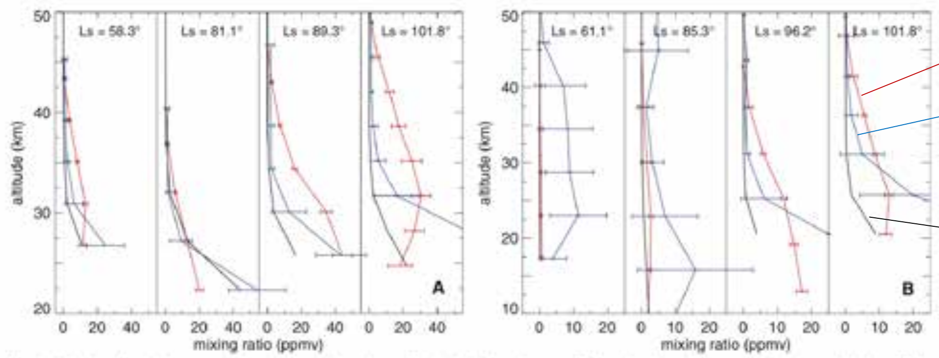

Observation

Saturation pressure

Model

Fig. 2. Selection of typical water vapor volume-mixing ratio profiles in the (**A**) northern and (**B**) southern hemisphere. Black curve, modeled profile by the LMD-GCM; red curve, the retrieved SPICAM results; blue curve, saturation water vapor-mixing ratio. Supersaturation exists where the red values are greater than the blue ones.

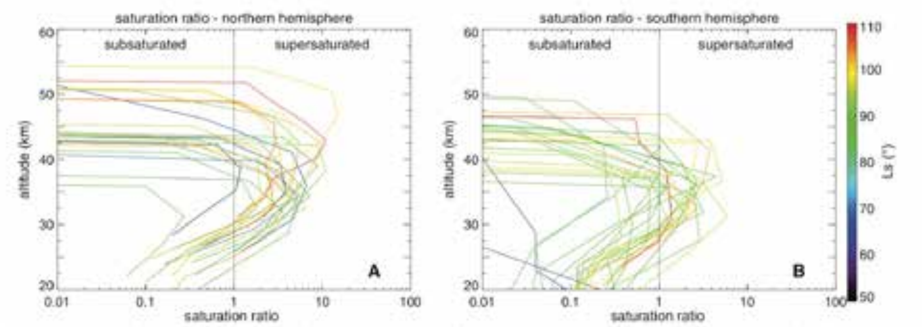

Fig. 3. Saturation ratio for all orbits of the campaign. (**A**) Northern hemisphere. (**B**) Southern hemisphere. The vertical line marks the value of 1, which corresponds to the saturated state.

Dependence of volatile escape on lower atmosphere processes

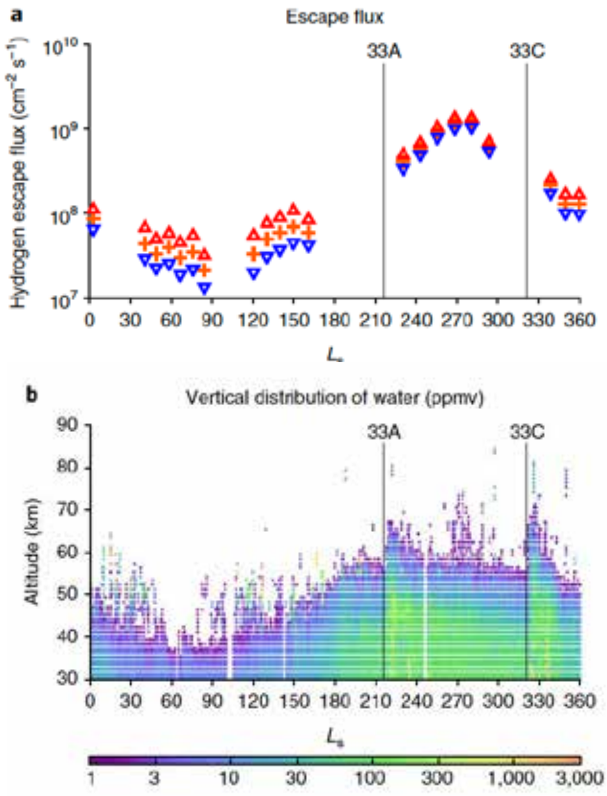

Hydrogen escape measured by MAVEN Solar Wind Ion Analyzer

Vertical distribution of total water content measured by MRO MCS

Heavens et al. (2018)

Meridional cross sections in Mars GCM (Shaposhnikov et al. 2019)

Meridional distribution of zonal-mean temperature obtained by MGS/TES (Smith et al. 2001)

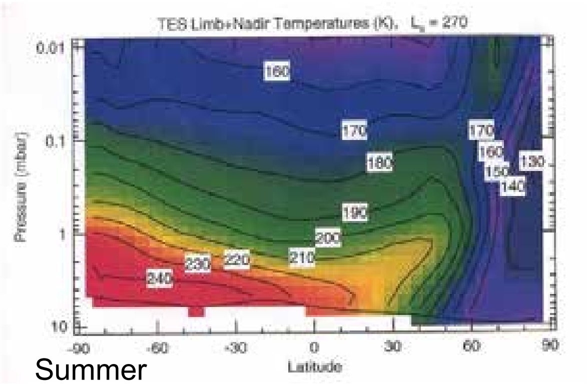

Summer
Winter

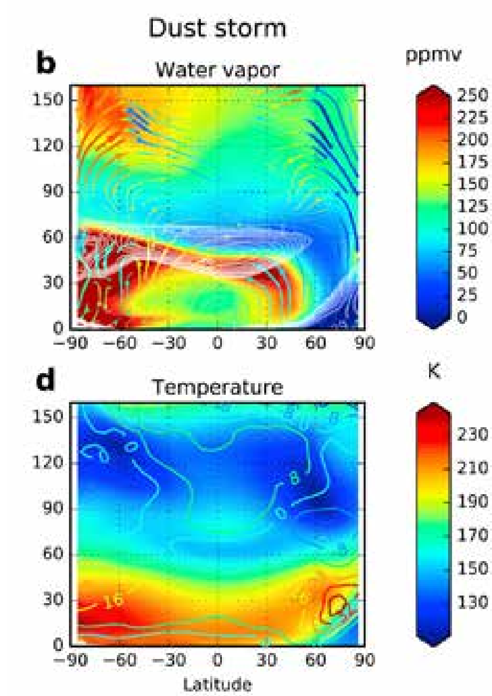

Traditional scheme New concept

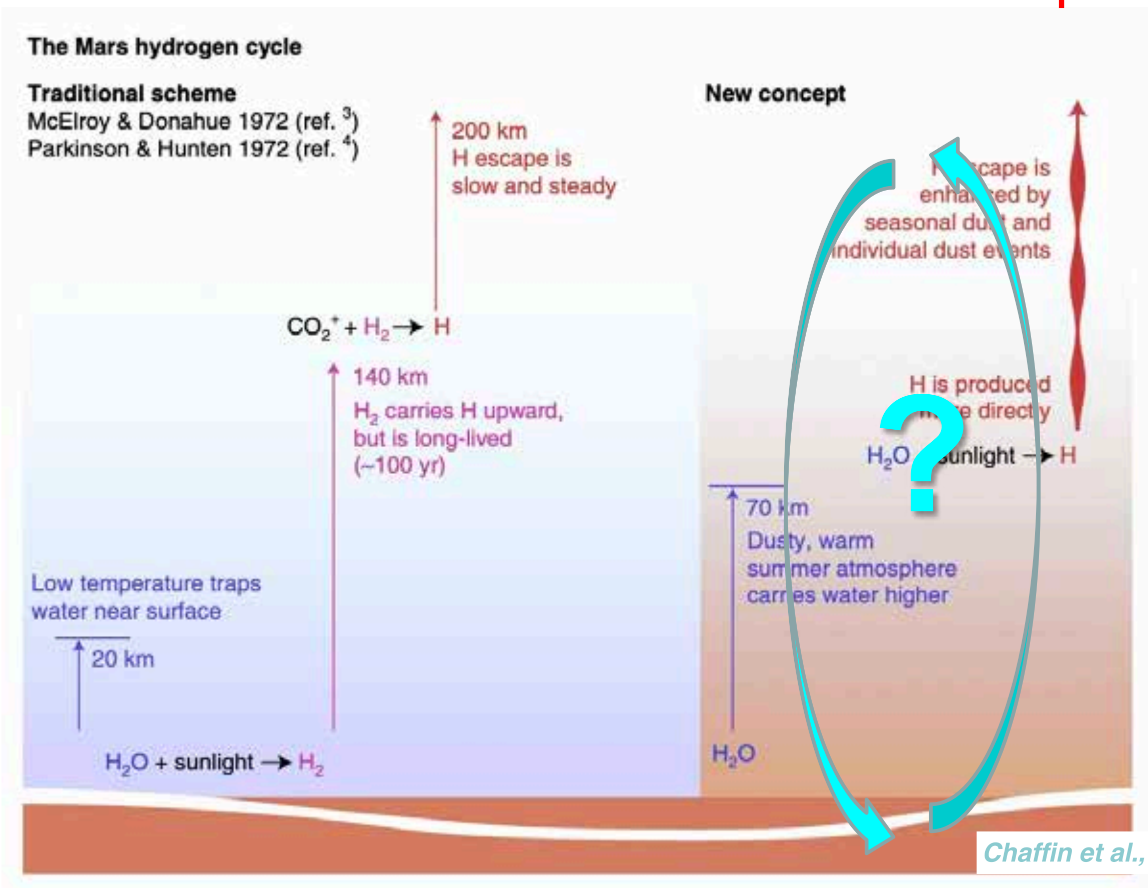

Chaffin et al., 2021

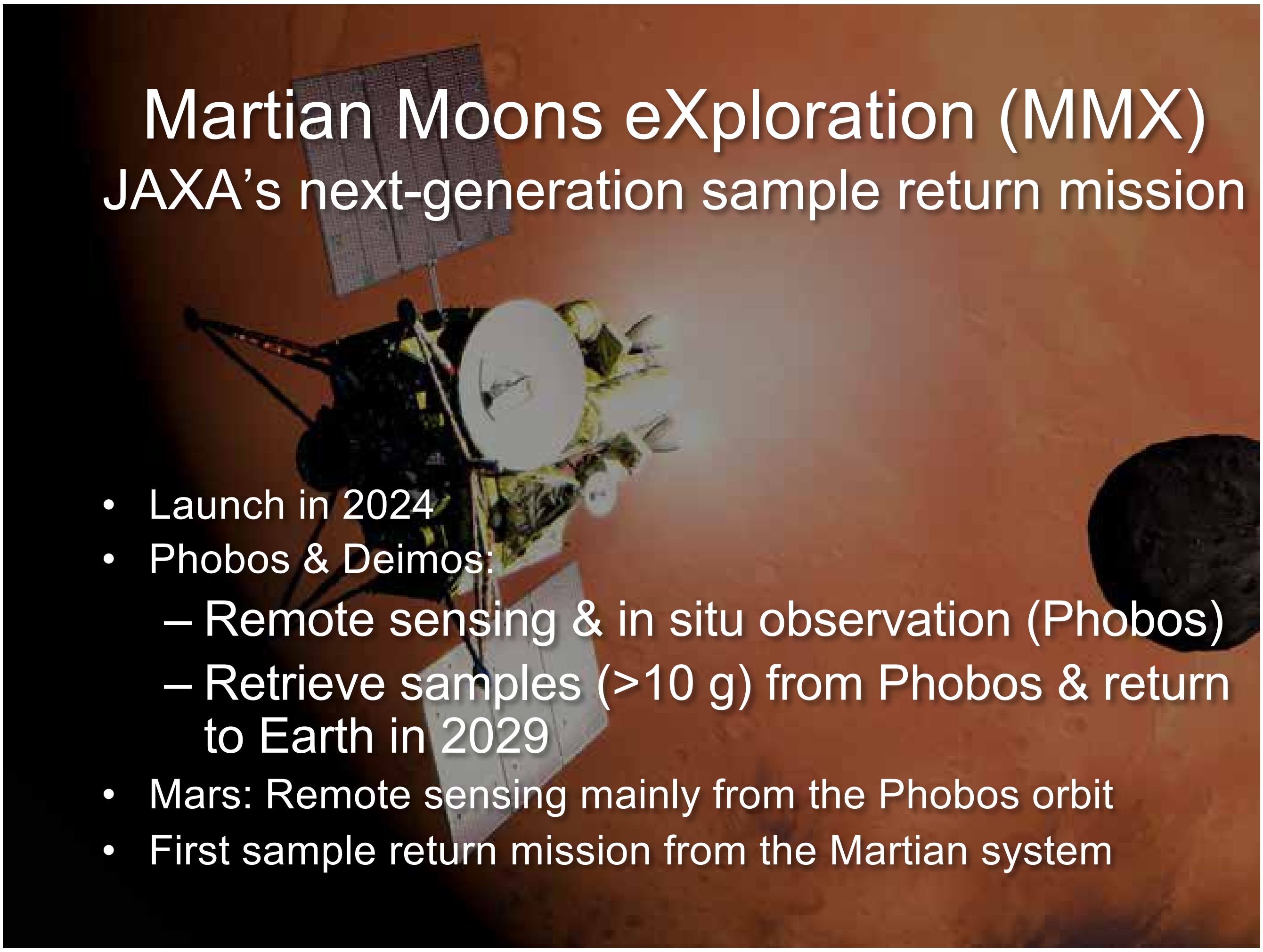

Martian Moons eXploration (MMX)

JAXA's next-generation sample return mission

- Launch in 2024
- Phobos & Deimos:
  - Remote sensing & in situ observation (Phobos)
  - Retrieve samples (>10 g) from Phobos & return to Earth in 2029
- Mars: Remote sensing mainly from the Phobos orbit
- First sample return mission from the Martian system

Instruments for Mars atmosphere observation

- **OROCHI**
  - Wide-angle camera, 8 colors
  - 3 colors (480, 650, 950 nm) will be used for Mars observation.
  - 2.5 km/pix (sub S/C) from QSO
- **TENGOO**
  - Narrow-angle camera
  - 35 m/pix (sub S/C) from QSO
- **MIRS**
  - Push-bloom type spectrometer
  - Spectral resolution: 10nm
  - Spectral bandpass: 0.9–3.6 μm
  - 2.1 km/pix (sub S/C) from QSO

Kameda et al. (2021)

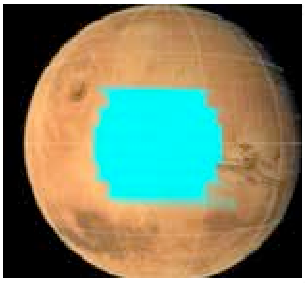

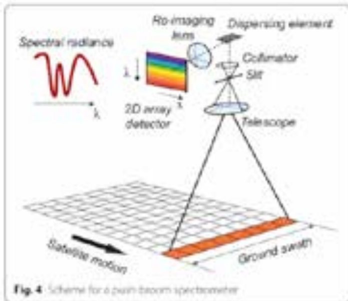

Barucci et al. (2021)

Continuous global monitoring from Martian orbit

High-altitude equatorial orbit is a unique platform for atmospheric studies

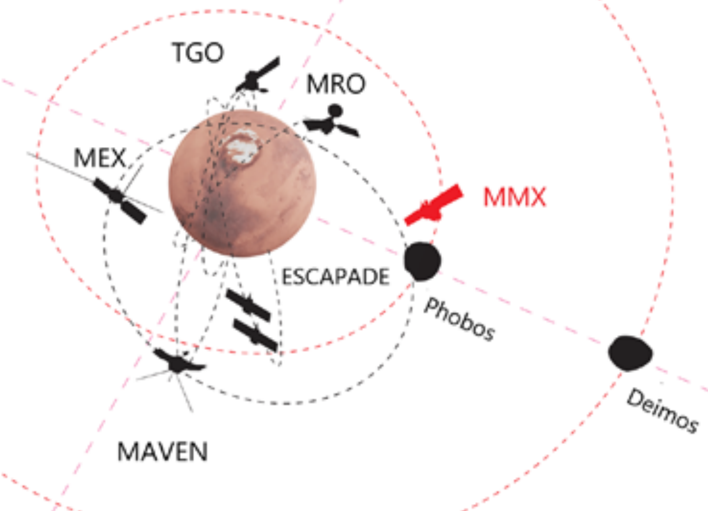

Ogohara et al. (2022)

Venus images taken by JAXA's Akatsuki

UV

IR

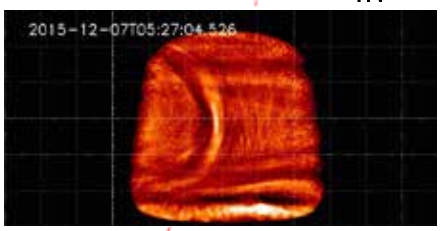

Mars Odyssey

Neutron Spectrometer (NS) and High-Energy Neutron Detector (HEND)

Subsurface ice

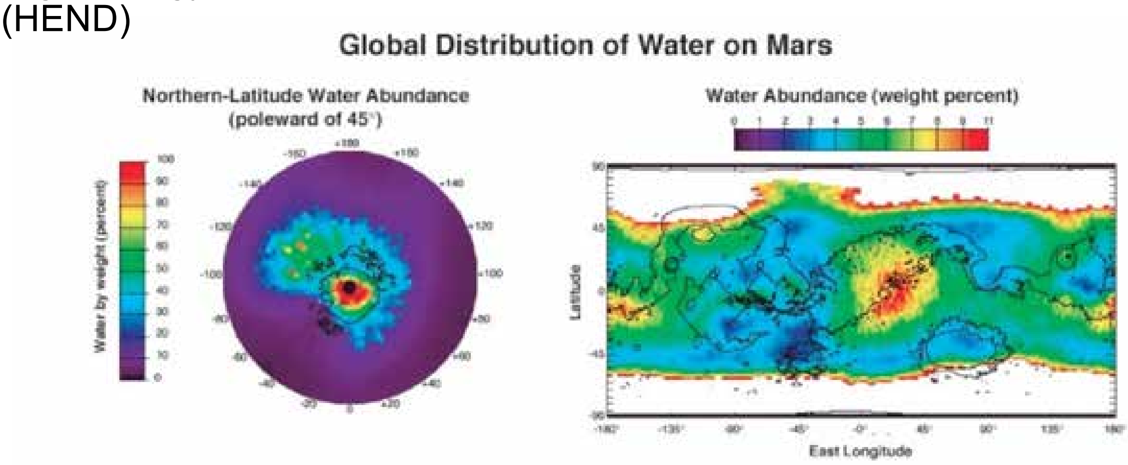

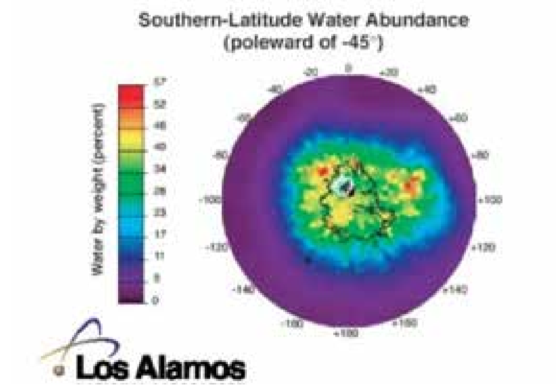

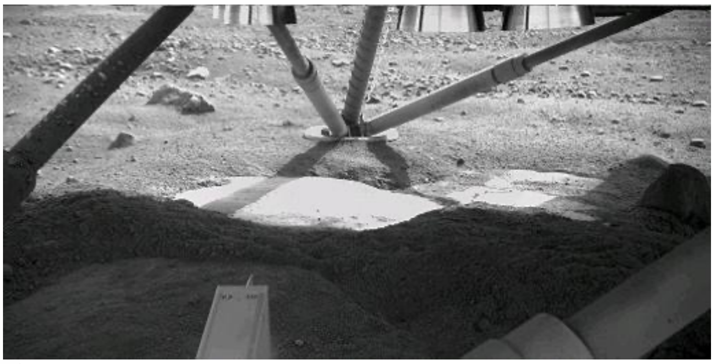

Phoenix Mars Lander

Chemistry of gas giants

Many of the gases in the gas giants are hydrides, which are thermodynamically stable (e.g., CH_4, NH_3, H_2O, H_2S, PH_3, GeH_4, and AsH_3).

These gases (except H_2O and H_2S) are photochemically destroyed by solar UV to produce disequilibrium species (e.g., ethane C_2H_6, ethylene C_2H_4, acetylene C_2H_2, hydrazine N_2H_4).

The disequilibrium species react with H_2 to reform hydrides once they are transported downward into the hot, high pressure regions.

Lodders, 2010

Table 2. *Composition of the Atmospheres of Jupiter, Saturn, Uranus, and Neptune*

Gas	Jupiter[a]	Saturn	Uranus	Neptune
H_2	86.4 ± 0.3%	88 ± 2%	~82.5 ± 3.3%	~80 ± 3.2 %
^4He	13.6 ± 0.3%	12 ± 2%	15.2 ± 3.3 %	19.0 ± 3.2 %
CH_4	$(1.81 \pm 0.34) \times 10^{-3}$	$(4.7 \pm 0.2) \times 10^{-3}$	~2.3 %	~1-2 %
NH_3	$(6.1 \pm 2.8) \times 10^{-4}$	$(1.6 \pm 1.1) \times 10^{-4}$	<100 ppb	<600 ppb
H_2O	520^{+340}_{-240} ppm	2–20 ppb		
H_2S	67 ± 4 ppm	<0.4 ppm	<0.8 ppm	<3 ppm
HD	45 ± 12 ppm	110 ± 58 ppm	~148 ppm	~192 ppm
$^{13}CH_4$	19 ± 1 ppm	51±2 ppm		
C_2H_6	5.8 ± 1.5 ppm	7.0 ± 1.5 ppm		
PH_3	1.1 ± 0.4 ppm	4.5 ± 1.4 ppm		
CH_3D	0.20 ± 0.04 ppm	0.30 ± 0.02 ppm	~8.3 ppm	~12 ppm
C_2H_2	0.11 ± 0.03 ppm	0.30 ± 0.10 ppm	~10 ppb	60^{+140}_{-40} ppb
HCN	60 ± 10 ppb	<4 ppb	<15 ppb	0.3 ± 0.15 ppb
HC_3N			<0.8 ppb	<0.4 ppb
C_2H_4	7 ± 3 ppb	~0.2 ppb[b]		
CO_2	5-35 ppb	0.3 ppb	40 ± 5 ppt	
C_2H_6			10 ± 1 ppb	$1.5^{+2.5}_{-0.5}$ ppm
CH_3C_2H	2.5^{+2}_{-1} ppb	0.6 ppb	0.25 ± 0.03 ppb	
CO	1.6 ± 0.3 ppb	1.4 ± 0.7 ppb	<40 ppb	0.65 ± 0.35 ppm
CH_3CN				<5 ppb
GeH_4	$0.7^{+0.4}_{-0.2}$ ppb	0.4 ± 0.4 ppb		
C_4H_2	0.3 ± 0.2 ppb	0.09 ppb	0.16 ± 0.02 ppb	
AsH_3	0.22 ± 0.11 ppb	2.1 ± 1.3 ppb		

[a] ^3He 22.6±0.7 ppm, Ne 21±3 ppm, Ar 16±3 ppm, Kr 8±1 ppb, Xe 0.8±0.1 ppb.

[b] assuming a total stratospheric column density of 1.54%10^{25} cm^{-2}.

From Lodders & Fegley 1998 and updates: Mahaffy et al. 2000, Atreya et al. 2003, Lodders 2004, Wong et al. 2004

Chemical cycle of hydrogen-bearing species in giant planets

Catling & Kasting (2017)

$$2CH_4 + \text{photons} \rightarrow \underbrace{C_2H_6 + H_2}_{\text{ethane + hydrogen}}$$

$$2nCH_4 + \text{photons} \rightarrow \underbrace{(C_2H_2)_n + 3nH_2}_{\text{polyacetylene + hydrogen}}$$

$$6nCH_4 + \text{photons} \rightarrow \underbrace{(C_6H_6)_n + 9nH_2}_{\text{polyaromatic hydrocarbons + hydrogen}}$$

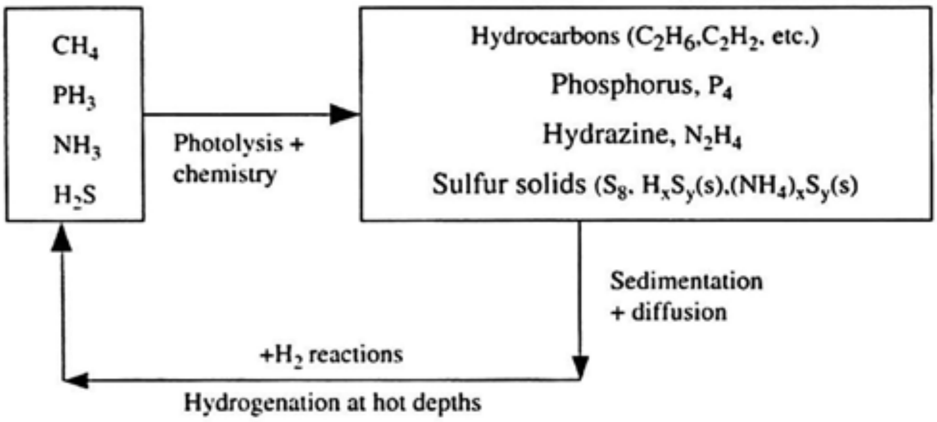

Clouds of Jupiter and Saturn

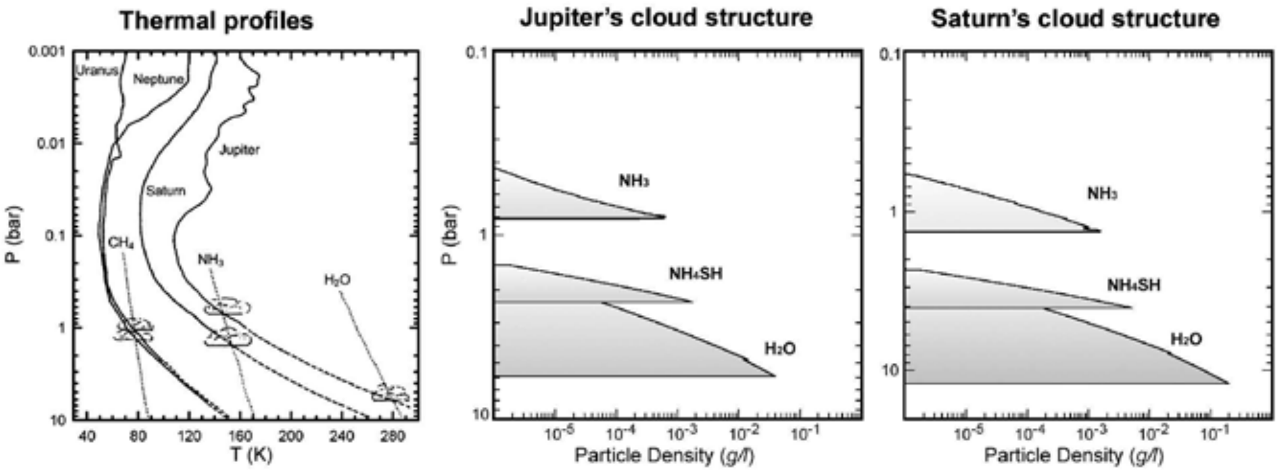

Sanchez-Lavega et al.

Galileo probe (entry: December 7, 1995)

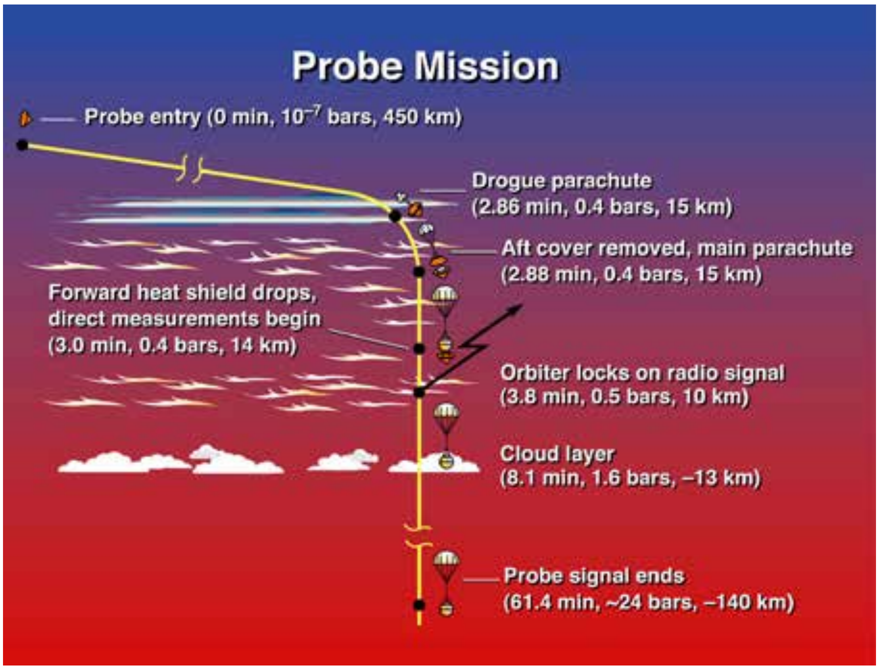

Dry atmosphere ?

- Brightness of the sky abruptly drops off at a pressure level of 0.6 bars, indicating an **ammonia cloud layer** above this height. The tenuous cloud layer detected by the NEP was *not* seen by this experiment.
- **Clouds are patchy and that the Probe went through a relatively clear area**.
- **The atmosphere has much less oxygen than the Sun's atmosphere, implying a surprisingly dry atmosphere.**
- Planetary scientists had expected **oxygen** to be enriched relative to the solar value due to impacts by comets and other small bodies over the 4.5 billion years.

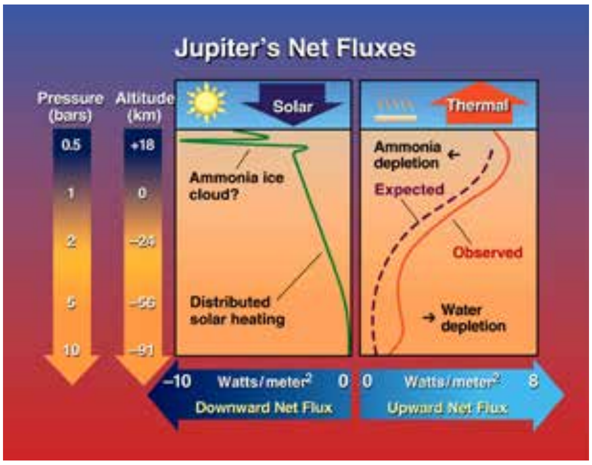

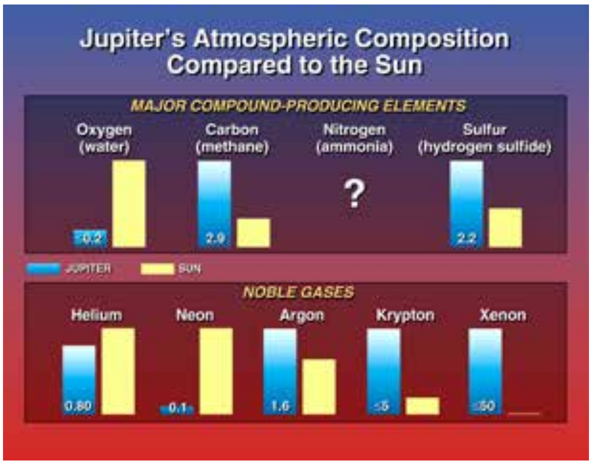

The probe apparently entered a special location

The Probe entry site is near the edge of a so-called infrared "**hot spot**". These "hot spots" are believed to represent regions of diminished clouds on Jupiter.

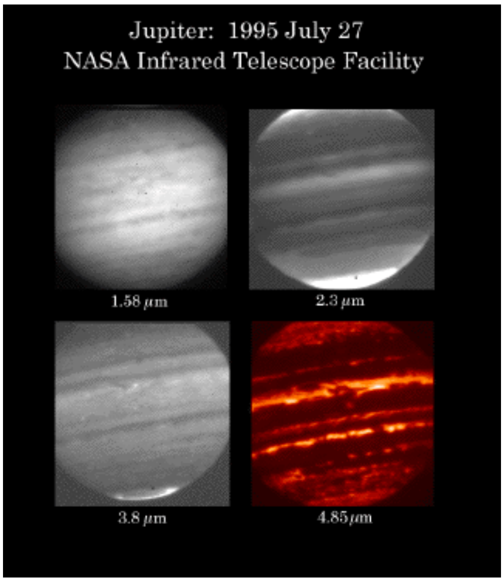

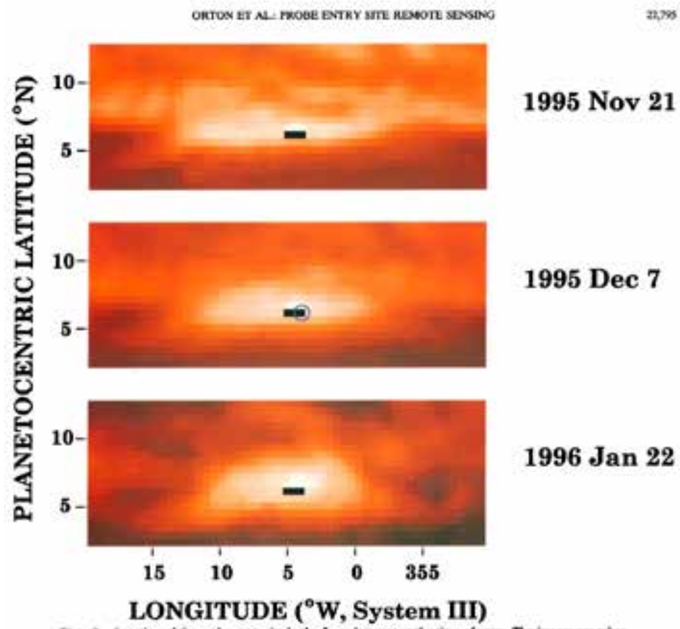

Plate 3. Location of the probe entry site in the 5-μm hot spot at the time of entry. The images are taken from the upper panel of Plate 2 and, again, scaled to the brightest pixel in each image. A single 0.5° × 0.5° pixel is used to denote the 6.5°N planetocentric latitude and System III longitude of the probe entry, and a 1.5° longitude (three-pixel) extent depicts the longitudinal extent of the probe entry path, starting from 350 km above the 1-bar level to the 1-bar level and deeper (as in Figures 1 and 2 of *Orton et al.* [1996]) A 1-σ circle shows the effects of the pointing uncertainty on the location of the final portion of the probe entry. The panels from different dates were aligned together using a drift rate of 103 m/s relative to System III.

Orton et al. 1998

Atmospheric chemistry on Titan

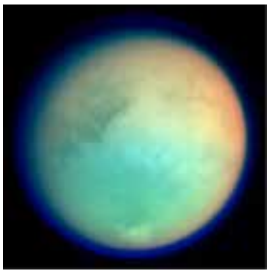

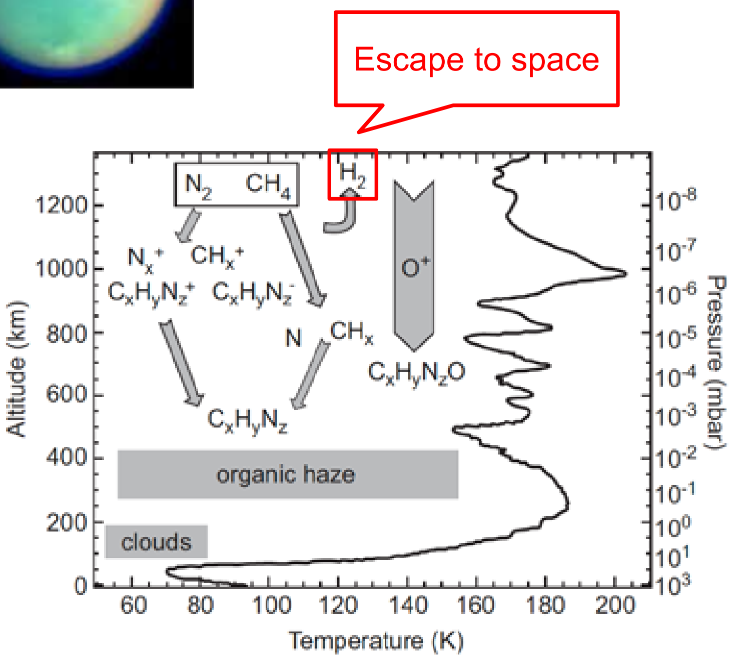

Vuitton et al. (2014)

Atmospheric composition of Titan (Coustenis 2007)

Constituent	Mole Fraction (atm. altitude level)
Major	
Molecular nitrogen, N_2	0.98
Methane, CH_4	4.9×10^{-2} (surface)
	$1.4–1.6 \times 10^{-2}$ (stratosphere)
Monodeuterated methane, CH_3D	6×10^{-4} (in CH_3D, in stratosphere.)
Argon, ^{36}Ar	2.8×10^{-7}
^{40}Ar	4.3×10^{-5}
Minor	
Hydrogen, H_2	~0.0011
Ethane, C_2H_6	1.5×10^{-5} (around 130 km)
Propane, C_3H_8	5×10^{-7} (around 125 km)
Acetylene, C_2H_2	4×10^{-6} (around 140 km)
Ethylene, C_2H_4	1.5×10^{-7} (around 130 km)
Methylacetylene, CH_3C_2H	6.5×10^{-9} (around 110 km)[a]
Diacetylene, C_4H_2	1.3×10^{-9} (around 110 km)[a]
Cyanogen, C_2N_2	5.5×10^{-9} (around 120 km)[a]
Hydrogen cyanide, HCN	1.0×10^{-7} (around 120 km)[a]
	5×10^{-7} (around 200 km)[b]
	5×10^{-6} (around 500 km)[b]
Cyanoacetylene, HC_3N	1×10^{-9} (around 120 km)[c]
	1×10^{-7} (around 500 km)[b]
Acetonitrile, CH_3CN	1×10^{-8} (around 200 km)[c]
	1×10^{-7} (around 500 km)
Water, H_2O	8×10^{-9} (at 400 km)[d]
Carbon monoxide, CO	4×10^{-5} (uniform profile)[e]
Carbon dioxide, CO2	1.5×10^{-8} (around 120 km)

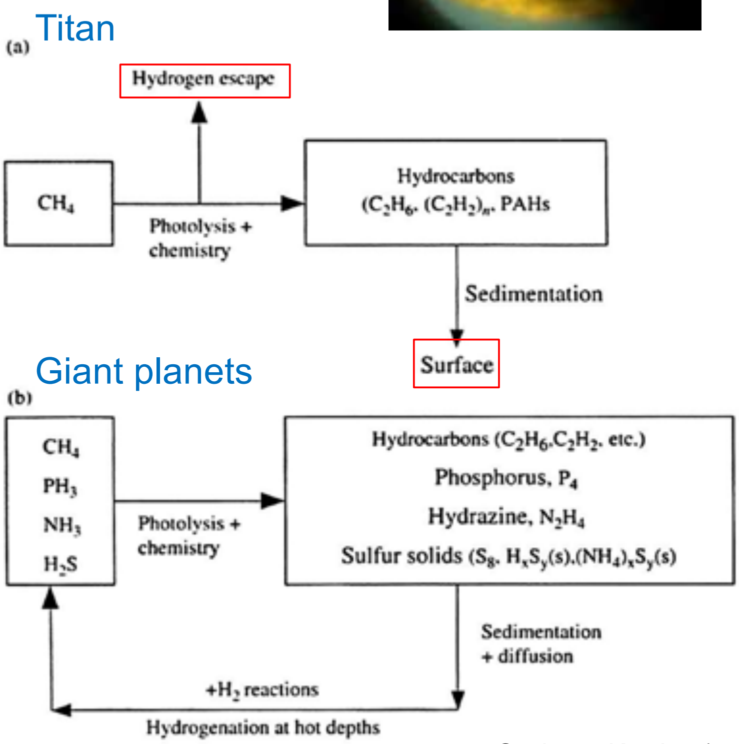

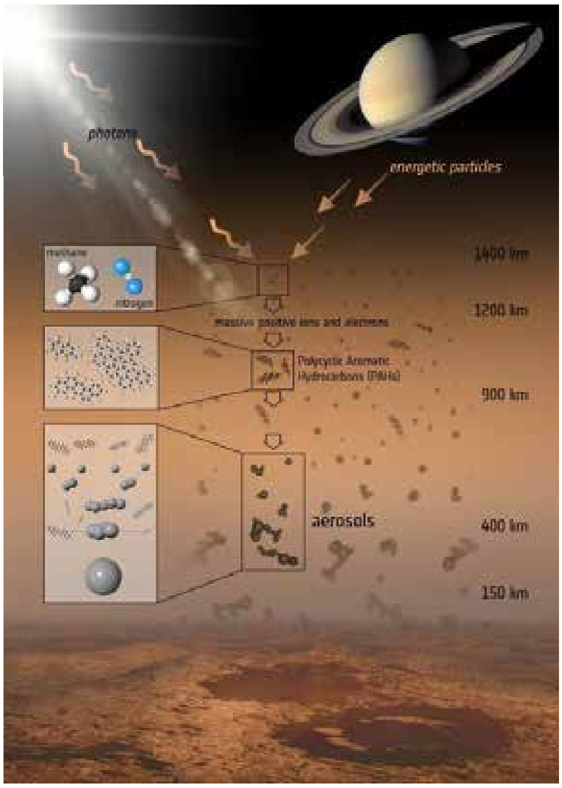

© NASA

Catling & Kasting (2017)

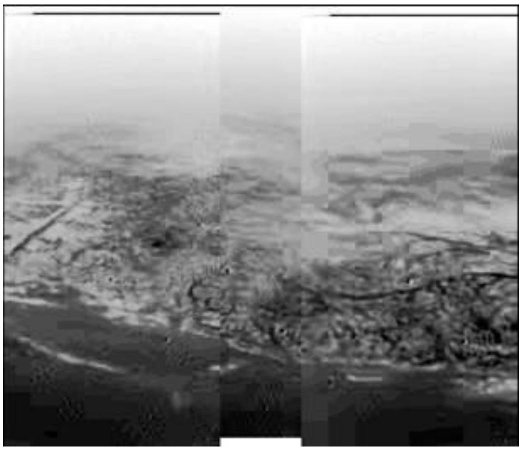

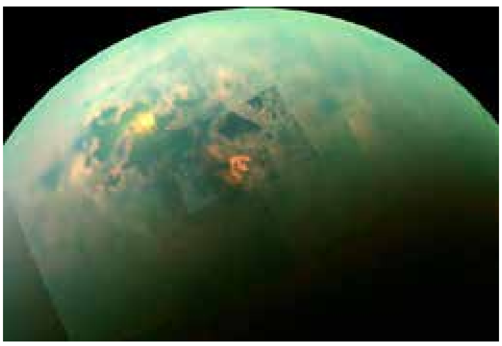

Cassini's Visual and Infrared Mapping Spectrometer (VIMS)

Huygens' touchdown